

# A Neuro-Symbolic Framework Combining Inductive and Deductive Reasoning for Autonomous Driving Planning

Hongyan Wei, Wael AbdAlmageed

Clemson University

**Abstract.** Existing end-to-end autonomous driving models rely heavily on purely data-driven inductive reasoning. This “black-box” nature leads to a lack of interpretability and absolute safety guarantees in complex, long-tail scenarios. To overcome this bottleneck, we propose a novel neuro-symbolic trajectory planning framework that seamlessly integrates rigorous deductive reasoning into end-to-end neural networks. Specifically, our framework utilizes a Large Language Model (LLM) to dynamically extract scene rules and employs an Answer Set Programming (ASP) solver for deterministic logical arbitration, generating safe and traceable discrete driving decisions. To bridge the gap between discrete symbols and continuous trajectories, we introduce a decision-conditioned decoding mechanism that transforms high-level logical decisions into learnable embedding vectors, simultaneously constraining the planning query and the physical initial velocity of a differentiable Kinematic Bicycle Model (KBM). By combining KBM-generated physical baseline trajectories with neural residual corrections, our approach inherently guarantees kinematic feasibility while ensuring a high degree of transparency. On the nuScenes benchmark, our method comprehensively outperforms the state-of-the-art baseline MomAD, reducing the  $L_2$  mean error to 0.57 m, decreasing the collision rate to 0.075%, and optimizing trajectory prediction consistency (TPC) to 0.47 m.

**Keywords:** Autonomous Driving Planning · Deductive Reasoning · Answer Set Programming · Kinematic Constraints

## 1 Introduction

Vision-based end-to-end autonomous driving systems aim to directly map raw sensor inputs to the vehicle’s planned trajectory using a unified neural network architecture. In recent years, end-to-end methods such as UniAD [13], VAD [15], and SparseDrive [25] have unified perception, prediction, and planning modules under a differentiable framework for joint optimization, continuously improving performance in benchmarks such as nuScenes [3]. MomAD [24] further introduces a trajectory momentum mechanism, achieving new breakthroughs in the temporal consistency of trajectories. However, this inductive reasoning paradigm, which relies entirely on massive amounts of training data, faces serious theoretical limitations: purely “black box” neural networks lack common-sense reasoning

capabilities and explicit physical and logical constraints. When faced with complex long-tail scenarios with out-of-distribution (OOD) training, the system can easily generate planned trajectories that defy common sense or even pose dangers. Furthermore, due to the lack of traceability in the internal decision-making process, researchers find it difficult to effectively attribute errors when trajectory planning fails.

Existing methods attempt to mitigate the aforementioned problems through two families of approaches, that both have fundamental limitations. The first approach directly regresses the displacement increment  $(\Delta x, \Delta y)$  of the trajectory. In this case, the neural network output is merely a numerical sequence in coordinate space, containing no physical semantics regarding acceleration intent or steering motivation. This produces trajectories that may be kinematically infeasible, unsafe or unconstrained by physical laws. The second approach addresses safety issues through post-processing, collision-re-scoring mechanisms [8, 25] or data augmentation methods [2, 15]. The former merely filters already-generated trajectories without affecting the trajectory generation process itself; the latter heavily relies on the coverage of the training data and cannot handle scenarios not included in the training set. Neither family alters the planner’s purely inductive-reasoning nature, and thus failing to guarantee the rationality of the planning behavior at a logical level.

To address this dilemma, traditional solutions typically resort to purely symbolic systems or rule-based expert systems [21] (*i.e.* pure deductive reasoning). However, purely symbolic methods are limited by the enumeration capacity of manually formulated rules and cannot handle the complex semantic information in real-world traffic environments. Furthermore, symbolic reasoning produces discrete driving commands. Transforming these discrete commands into continuous trajectories that satisfy kinematic constraints is itself a significant challenge. On the other hand, methods that directly utilize large language models for end-to-end reasoning and decision-making, while possessing powerful semantic understanding capabilities, cannot guarantee the logical consistency of the reasoning results and lack physical constraints on kinematic feasibility.

In fact, the reasoning and decision-making processes of human drivers provide an excellent insights for solving these problems. While driving, humans do not rely solely on instinctive pattern matching (*i.e.* inductive reasoning). Instead, humans often complement the strengths of both intuition and logic. Specifically, humans use neural network-like intuition to handle complex environmental interactions, while simultaneously using traffic rules and common sense as a rigorous logical basis for deduction. Inspired by this, this paper proposes a novel paradigm for autonomous driving trajectory planning. This paradigm deeply integrates deductive reasoning from classical artificial intelligence with inductive reasoning from modern deep learning, thus constructing a neuro-symbolic planning framework. This framework not only possesses powerful feature representation capabilities but also rigorous interpretability. To achieve this goal, we must address two key technical challenges: First, how to meaningfully apply the discrete decisions (including actions and target velocities) produced by deductive

reasoning to the continuous trajectory decoding process of the neural planner? Second, how to ensure that the trajectory representation of the neural planner possesses sufficient physical semantics, so that the target velocity produced by deductive reasoning can directly and accurately constrain the velocity curve of the final trajectory.

To address the aforementioned challenges, this paper proposes an end-to-end autonomous driving framework that integrates inductive and deductive reasoning. This framework utilizes Large Language Models (LLM) and Answer Set Programming (ASP) to construct an explicit logical reasoning path, dynamically embedding the generated discrete decisions into the feature space of the neural planner. Simultaneously, we introduce a differentiable kinematic bicycle model (KBM) to establish a physical trajectory decoding paradigm with residual correction. This design successfully bridges the semantic gap between discrete symbolic logic and continuous physical space—physical trajectory representation not only naturally guarantees the kinematic feasibility of the trajectory but also provides the physical premise for precisely constraining the velocity curve of the trajectory through deductive decision-making.

Compared to purely inductive planning methods [13,25], our approach generates logically-based planning behavior without relying on the coverage of training data. Compared to purely symbolic methods [21] or methods that directly use large language models [9,14,28], this method retains the powerful perceptual generalization ability of neural networks while using Clingo [10] solvers and KBM models to ensure the logical consistency of reasoning and the physical feasibility of trajectories. In summary, the main contributions of this paper are as follows:

1. **Embedded Neuro-Symbolic Planner.** To the best of our knowledge, this is the first work to directly apply ASP symbolic reasoning decisions to the end-to-end planner trajectory decoding process in a learnable embedding form, which is fundamentally different from the passive filtering applied after trajectory generation in existing methods.
2. **Decision-Conditioned Physical Residuals.** We replace the direct displacement regression method with a differentiable KBM to generate a physical baseline trajectory that satisfies kinematic constraints. Simultaneously, we fine-tune the trajectory using residual predictions from the neural network output to compensate for modeling errors in the physical model. These physical control quantities provide semantically consistent access points for ASP target velocity decisions.
3. **Dynamic LLM-ASP Reasoning Engine.** We use a large language model as a scene-adaptive rule extractor and Clingo as a formal logic solver, thereby achieving open semantic reasoning that goes beyond a fixed rule base. We designed a five-level priority arbitration layer to formally encode the constraint hierarchy of traffic rules. This enables the system to generate unique and traceable driving decisions for any perceptual input.

The remaining sections of this paper are organized as follows: Section 2 reviews related work, Section 3 details the proposed method, Section 4 reports experimental results and analysis, and Section 5 summarizes the entire paper.

## 2 Related Work

### 2.1 End-to-End Autonomous Driving Planning

End-to-end autonomous driving has seen rapid progress in recent years [5]. Early end-to-end planning methods relied primarily on imitation learning, directly regressing driving control variables from sensor inputs [4, 29]. In recent years, with the rise of Transformer architecture [7, 16, 19] and multi-task learning, the capabilities of end-to-end planning methods have been significantly expanded [12, 20]. UniAD [13] unifies perception, prediction, and planning within a single differentiable framework for joint optimization; VAD [15] introduces vectorized scene representations to improve efficiency; SparseDrive [25] achieves a better balance between speed and accuracy with a symmetric sparse perception architecture; and MomAD [24] introduces a trajectory momentum mechanism to improve temporal consistency. Essentially, these methods all inductively map a statistical relationship from perception to trajectory from training data. Their performance ceiling is highly dependent on data coverage and lacks the ability to utilize the logical patterns of complex scenarios.

### 2.2 LLM-Based Planning

Large language models have recently emerged as a promising direction for autonomous driving, offering strong common-sense reasoning and zero-shot generalization capabilities that purely data-driven methods inherently lack [9, 31]. The powerful common-sense reasoning capabilities of large language models have spurred research into LLM-driven driving decisions [9]. DriveGPT [14], DriveGPT4 [30] and DriveMLM [28] utilize the language reasoning capabilities of LLMs to directly generate driving actions or trajectories, while DriveLM [23] combines driving question answering with a visual-language model [17] to construct a chain-like reasoning framework. DriveVLM [26] proposes a chain-of-thought reasoning pipeline combining scene description, scene analysis, and hierarchical planning, and further introduces a slow-fast hybrid system to bridge VLM latency and real-time control requirements. These methods possess strong semantic understanding capabilities and a certain degree of zero-shot generalization. However, the generation process of LLMs lacks consistency guarantees in formal logic, potentially leading to contradictory decisions under different invocations of the same input. Furthermore, natural language instructions still require additional mechanisms to be transformed into continuous physical trajectories that satisfy kinematic constraints.

### 2.3 Deductive Reasoning and Symbolic Methods in Planning

Introducing deductive reasoning into autonomous driving planning is a direct way to improve the logical rationality of planning behavior. Early symbolic planning methods (such as expert systems) [21] are logically rigorous but have limited scalability and cannot handle the semantic complexity of real traffic. Recent

work attempts to combine neural perception with rule engines: some methods let the rule engine judge the scene features extracted by the neural network, while others use symbolic constraints to post-process and correct the neural output. The common structural feature of these methods is that deductive reasoning and trajectory generation are “serialized”—the conclusions of symbolic reasoning only affect the downstream of the neural network output and cannot directly participate in the trajectory decoding process itself. Sharifi et al. [22] combine symbolic logical programming with deep reinforcement learning to enforce safety constraints in highway driving, demonstrating that logic-guided policy learning can reduce collision rates in structured environments. In the broader field of neural symbolic learning, frameworks such as DeepProbLog [18] have explored methods of embedding logical rules into network training, but these have not yet been validated in complex 3D perception-driven real-time planning scenarios.

## 2.4 Physics-Constrained Trajectory Planning

Introducing physical model constraints into learning-based planning is an effective way to improve trajectory feasibility. Kinematic bicycle models (KBMs) are computationally simple and can capture the core features of vehicle steering dynamics, making them widely used in model predictive control (MPC) and traditional motion planning. Recent work has embedded KBMs in a differentiable form into deep learning frameworks: KING [11] and PlanTF [6] utilize physical models to generate trajectory candidates for neural network scoring, but the control variables themselves do not participate in end-to-end feature learning. Physical rule-based car-following models such as IDM [27] demonstrate the accuracy of symbolic methods in longitudinal speed control, but lack adaptability to complex dynamic interaction scenarios. In stark contrast to the above methods, this paper fully embeds KBMs into the planning decoder and participates in system optimization through gradient backpropagation. More importantly, KBM provides a direct physical access point for velocity bias in the deductive decision (target velocity) of this paper, a mechanism design that is not available in existing methods.

# 3 Method

## 3.1 Overall Architecture

As illustrated in Fig.1, the neural symbol trajectory planning framework proposed in this paper consists of three core modules: (1) Perception Fact Extraction: extracting structured representations of 3D targets, and mapping topology and other elements based on symmetric sparse perceptual networks; (2) Dynamic Deductive Reasoning Engine: dynamically generating scene-specific ASP rules using a large language model (LLM), and performing strict logical arbitration through a Clingo solver to produce the optimal high-level discrete decision; (3) Decision-Conditioned Physical Residual Planner: transforming high-level decisions into control parameters of the physical baseline trajectory and neural network residuals to generate the final continuous trajectory.

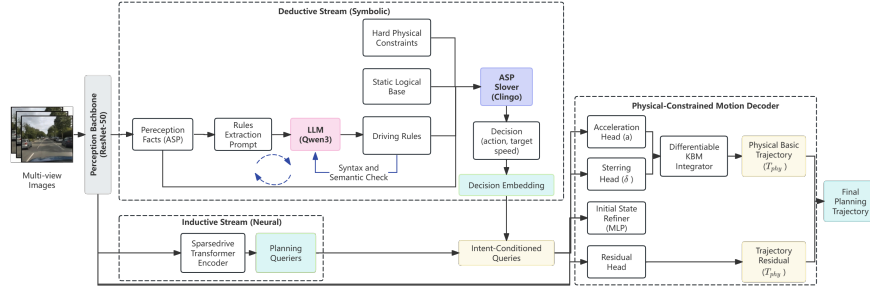


**Fig. 1:** Overall framework. The inductive stream (neural) and deductive stream (symbolic) run in parallel. The ASP engine produces discrete driving decisions which are conditioned into the Physics-Constrained Motion Decoder via dual paths: Path 1 modulates planning queries  $\mathbf{Q}'_{\text{plan}} = \mathbf{Q}_{\text{plan}} \oplus \mathbf{d}$  (spatial shape), and Path 2 biases the KBM initial velocity  $v'_0 = v_0 + b_v$  (speed profile).

### 3.2 Deductive Reasoning via LLM and ASP

To incorporate human experts' traffic rules and common sense about physics into the system, we built a deductive reasoning engine based on Answer Set Programming (ASP). As illustrated in Fig.2, this engine operates in two sequential stages: dynamic rule extraction via an LLM, followed by deterministic arbitration using an ASP solver.

*Scene Fact Formulation.* The output of the underlying perception module is structured into strict ASP predicates. For example, dynamic obstacles are represented as predicates with precise parameters: *object(id, category, distance, speed, heading, relative\_pos, attribute, etc)*. Vehicle state and history information are also converted into ego facts accordingly.

*LLM-Based Rules Extraction.* Hand-crafted rules often struggle to encompass the extensive long-tail of real-world traffic scenarios. To overcome this limitation, we design a structured System Prompt (see "Prompt" in Fig. 2) that defines the LLM's role as an "autonomous driving rule and ASP programming expert." Conditioned on the extracted semantic facts, the LLM dynamically generates 3 to 6 ASP logic suggestions tailored to the specific context of the current frame. This generation process is governed by expert prior knowledge and rigorous syntactic constraints (e.g., predicate formatting and variable safety). To ensure seamless logical arbitration, the output is strictly standardized as *suggestion(Action, TargetSpeed, Type)*. Here, *Type* characterizes the underlying rationale of the generated rule, such as an *emergency* intervention, a *safety* precaution, or *legal* compliance. The precise definitions and boundaries of the remaining driving state variables (*Action* and *TargetSpeed*) are strictly constrained by a pre-defined symbolic vocabulary, as detailed below.

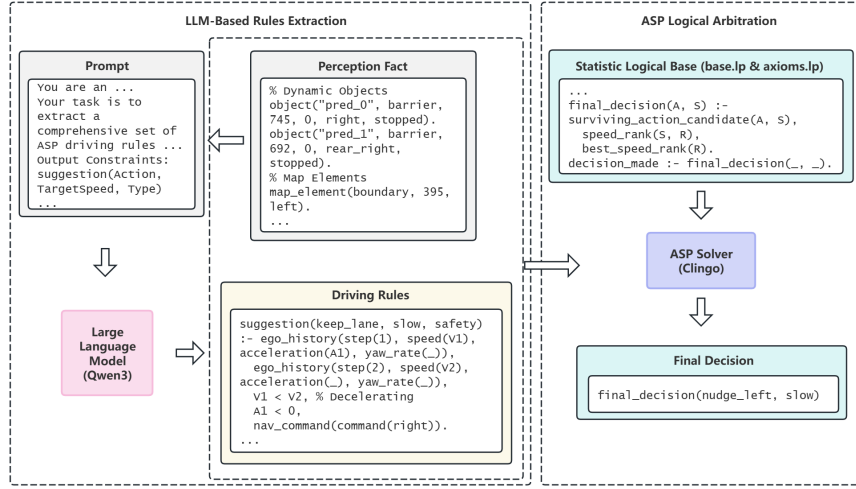


**Fig. 2:** Detailed pipeline of the deductive reasoning engine. The LLM extracts semantic rules from perception facts via prompts, which are then combined with a static logical base and evaluated by the ASP solver (Clingo) to deduce final deterministic driving decisions.

*Symbolic Vocabulary Design.* To ensure deterministic logical arbitration and eliminate semantic ambiguity, we carefully construct a compact, mutually exclusive symbolic vocabulary tailored for complex urban driving. Rather than allowing free-form language generation, the LLM’s output is strictly constrained to this pre-defined semantic space. This vocabulary is systematically distilled from expert driving knowledge to maximize expressiveness while ensuring zero redundancy or semantic overlap. Specifically, the vocabulary encompasses:

- (1) Action (9 states): `keep_lane`, `change_lane_left`, `change_lane_right`, `turn_left`, `turn_right`, `nudge_left`, `nudge_right`, `yield`, and `emergency_stop`.
- (2) Target Speed (6 levels): `current`, `zero`, `creep`, `slow`, `normal`, and `fast`.
- (3) Navigation Commands (3 modes): `left`, `right`, and `straight`.

By formally bounding the LLM outputs into this  $9 \times 6 \times 3$  discrete logical space, we strictly standardize the predicates as `suggestion(Action, TargetSpeed, Type)`, guaranteeing that every generated rule is logically parsable and actionable for the downstream ASP solver.

*ASP Logical Arbitration.* To ensure the uniqueness and absolute safety of the decision, dynamic rules are input into the Clingo solver along with predefined physical safety axioms (as shown in Fig. 2). In the logic library, we designed a strict categorical priority mapping to resolve conflicting rules: emergency avoidance represents the highest priority tier, followed by safety precautions as the medium tier, and finally regulatory compliance and efficiency goals. It is important to emphasize that this hierarchy does not rely on arbitrary hyperparameters

requiring network optimization; rather, it is a rigid formal encoding of the real-world traffic principle that “safety absolutely takes precedence over efficiency.” The solver evaluates facts and filters conflicting actions based on this hierarchical logic, logically outputting the globally optimal decision for the current frame: `final_decision(Action, Speed)`.

### 3.3 Decision-Conditioned Trajectory Generation

After obtaining absolutely safe discrete decision symbols, the core challenge is how to transform them into continuous control trajectories. To address this, we designed a physical residual programming module for decision conditionalization.

*Perception Backbone and Planning Queries.* The underlying perception module in this paper adopts the sparse perception architecture of SparseDrive [25], using ResNet-50 as the visual backbone network to extract 3D scene and map features. After spatiotemporal interaction, the perception network outputs a multimodal planning query, which is formally defined as:

$$\mathbf{Q}_{\text{plan}} \in \mathbb{R}^{B \times 1 \times M \times D}, \quad (1)$$

where  $B$  represents the batch size,  $M = 18$  represents the number of planning modes (6 trajectory candidates  $\times$  3 navigation commands), and  $D = 256$  represents the feature dimension. All subsequent contributing modules operate on  $\mathbf{Q}_{\text{plan}}$ , without altering the core perception backbone.

*Dual-Path Decision Embedding.* We first map discrete Actions and Speeds into high-dimensional decision feature vectors through an embedding layer. These features are then used to conditionally decode the trajectory via a dual-path mechanism: the first path injects the decision features as a semantic offset into the plan query to constrain the spatial shape of the trajectory; the second path learns a velocity bias parameter, which is directly used to correct the initial velocity of the physical model, thereby forcing the network to match the target velocity indicated by the underlying logic.

*Differentiable Kinematic Bicycle Model.* Existing end-to-end methods directly regress coordinate displacements, lacking physical constraints. We explicitly introduce a differentiable kinematic model (KBM) into the network decoder. Given the network-predicted acceleration  $a$  and front wheel steering angle  $\delta$ , the vehicle’s state at time step  $t$  is physically integrated using the second-order Runge-Kutta method (RK2):

$$\dot{x} = v \cos \psi, \quad \dot{y} = v \sin \psi, \quad \dot{v} = a, \quad \dot{\psi} = \frac{v \tan \delta}{L}, \quad (2)$$

where  $x$  and  $y$  denote the 2D spatial coordinates of the vehicle,  $v$  is the velocity,  $\psi$  represents the heading (yaw) angle,  $a$  is the acceleration,  $\delta$  is the front wheel steering angle, and  $L$  represents the vehicle’s wheelbase. The dot notation (e.g.,

$\dot{x}$ ) indicates the time derivative of the respective state variables. The model integrates the initial velocity after “velocity offset” correction to generate a baseline trajectory  $\tau_{\text{physics}}$  that perfectly conforms to vehicle dynamics constraints.

*Physics + Residual Prediction.* In real-world, complex dynamic interactions often cannot be perfectly fitted by ideal physical integrals alone. Therefore, the neural network, based on the physical baseline, further outputs a spatiotemporal residual  $\tau_{\text{residual}}$ . The final planned trajectory  $\tau_{\text{final}}$  is represented as:

$$\tau_{\text{final}} = \tau_{\text{physics}} + \lambda \cdot \tanh(\tau_{\text{residual}}). \quad (3)$$

In Eq. (3),  $\tau_{\text{physics}}$  provides a reliable baseline derived from physical priors, while the neural network predicts a spatiotemporal residual  $\tau_{\text{residual}}$  to account for complex multi-agent interactions. The tanh function is employed to bound the residual magnitude, and  $\lambda$  acts as a scaling factor to balance the contribution between the analytical baseline and the learned refinement. This residual design ensures that the final trajectory  $\tau_{\text{final}}$  remains physically plausible while being adaptive to dynamic environments.

To prevent residual terms from violating physical priors, we innovatively introduce an anisotropic residual loss function. In the loss function, we assign a penalty weight to the horizontal (Lateral/X-axis) residuals that is 10 times greater than that to the vertical (Y-axis) residuals, thereby strongly suppressing the physically inconsistent “sideslip” phenomenon. Furthermore, we incorporate control smoothing loss and auxiliary action classification loss to ensure that the feature space of the neural network always maintains a high degree of consistency with the high-level logical decisions.

### 3.4 Reasoning Chain: Traceable Planning via Deductive Reasoning

A key property of this framework is the generation of a complete inference chain during planning, from perceived facts to deductive decisions, from deductive decisions to physical control variables, and ultimately from control variables to the execution trajectory—all traceable throughout. Take a typical pedestrian yielding scenario as an example: the ASP engine infers from perceived facts that an insufficient Time-To-Collision (TTC) triggers the safety axiom, outputting a (yield, zero) decision after arbitration; the DecisionEmbedder transforms this into a negative velocity bias and a semantic planning query offset; the KBM then integrates the corrected initial velocity to generate a deceleration trajectory that strictly satisfies kinematic constraints.

This inference chain does not exist in a purely inductive planner. While an inductive baseline might also output a deceleration trajectory in a similar scenario through statistical pattern matching, it cannot provide any logical basis for “why” the deceleration occurs. The existence of our inference chain allows engineers to progressively review the precise logical basis of the planning behavior, offering independent value for system debugging and safety analysis.

## 4 Experiments

### 4.1 Experimental Setup

*Dataset and Metrics.* Experiments were conducted on the nuScenes dataset [3], which is currently the most authoritative and widely adopted benchmark in the field of autonomous driving (700/150/150 scenes for training, validation, and testing, 6 surround cameras, 2Hz sampling). To ensure a fair and objective comparison, we strictly adhere to the standard evaluation protocols universally accepted by the end-to-end autonomous driving community (*e.g.* UniAD [13], VAD [15], and SparseDrive [25]), rather than employing any custom metrics. Specifically, consistent with our primary baseline MomAD, we adopt three principal metrics to comprehensively evaluate planning performance: (1)  $L_2$  Error (m,  $\downarrow$ ): The  $L_2$  distance and its average ( $L_2$  Avg) between the predicted and ground truth trajectories at 1s, 2s, and 3s, measuring spatial accuracy. (2) Collision Rate (% ,  $\downarrow$ ): The proportion of frames where the predicted trajectory geometrically intersects with other bounding boxes, serving as the core safety metric. (3) Trajectory Prediction Consistency (TPC, m,  $\downarrow$ ): Proposed by MomAD, this measures the root mean square deviation between planned trajectories at adjacent time steps, evaluating temporal stability. It should be noted that nuScenes employs an open-loop evaluation protocol based on offline log replay. While this paradigm might inherently underestimate closed-loop collision risks and  $L_2$  error cannot fully capture dynamic driving quality, it remains the de facto standard benchmark for evaluating state-of-the-art end-to-end planners. Thus, we report our results under this protocol to maintain rigorous comparability with existing literature.

*Baselines and Implementation Details.* We select UniAD [13], VAD [15], SparseDrive [25], and MomAD [24] as our baselines. For a fair comparison, all methods use surround-view camera inputs and a ResNet-50 backbone (except UniAD). Our framework builds upon the SparseDrive-Small perception architecture (using an FPN with  $D = 256$ ,  $M = 18$ ) and adopts MomAD’s planning and training configurations. The training is decoupled into two stages. Stage 1 trains the KBM-constrained planner to establish a physical prior. Stage 2 introduces the ASP deductive conditioning, fine-tuning the model on the nuScenes training set for 10 epochs. We use the AdamW optimizer (initial learning rate of  $2 \times 10^{-4}$ ) with a batch size of 32 across 4 H200 GPUs. To accelerate training, ASP decisions (including fact encoding, LLM rules extraction, and Clingo solving) are pre-computed offline and indexed by their sample tokens.

For the deductive reasoning engine, we employ Qwen3 [1] to generate scene rules. In our offline benchmark evaluation, we execute the LLM frame-by-frame to explore the performance upper bound of the neuro-symbolic framework (the LLM rule extraction time is approximately 1 s per frame). However, to address real-time constraints in actual on-vehicle deployment, our framework inherently supports an asynchronous dual-rate mechanism: the computationally expensive LLM can run at a low frequency to extract macroscopic semantic rules, while

the lightweight Clingo solver executes high-frequency, frame-by-frame logical arbitration (under 5 ms per frame), seamlessly bridging the gap to real-time execution.

## 4.2 Main Results

Table 1 reports the comparison results on the nuScenes validation set. The results of the baseline methods are either obtained from their original papers or reproduced using official checkpoints, while the performance of our method is evaluated under identical settings.

Our method comprehensively outperforms the MomAD baseline across three core planning metrics: the  $L_2$  mean error decreases from 0.60 m to 0.57 m (5.0%), the collision rate drops from 0.09% to 0.075% (16.7%), and TPC improves from 0.54 m to 0.47 m (13.0%). The improvements in  $L_2$  and TPC reflect the synergistic effect of our two primary contributions: the KBM physics planner enhances the physical plausibility of the trajectory through bounded control constraints and temporal smoothing loss, while deductive decision conditionalization introduces scene adaptability based on logical inference. Furthermore, the significant reduction in collision rate demonstrates the effectiveness of the deductive reasoning path. Safety axioms (e.g., emergency braking, safe following) directly constrain the KBM integration via the target speed path, ensuring that planning behaviors in high-risk scenarios are rooted in rigorous logical inference rather than relying solely on the statistical coverage of the training data.

Analyzing the temporal progression of trajectory errors, the improvement in the short-term horizon (1 s: 12.9%, 2 s: 5.3%) is significantly more pronounced than in the long-term horizon (3 s: 1.1%). Compared with the Stage 1 variant (see Tab. 2, where 1 s  $L_2 = 0.27$  m), the deductive decision conditionalization yields measurable additional benefits in the short-term domain, indicating that the performance gain cannot be entirely attributed to the KBM alone. The immediate decision constraints provided by deductive reasoning (such as decelerating or yielding) tightly bound the immediate future states. The relatively smaller improvement in the long-term horizon perfectly aligns with the semantic scope of deductive reasoning: the ASP engine infers the immediate action intention for the current frame, whereas the trajectory shape at 3 s relies more heavily on the inductive generalization capability of the neural planner.

Compared to SparseDrive [25], our approach achieves significant improvements in  $L_2$  (0.57 m vs. 0.61 m) and TPC (0.47 m vs. 0.57 m) under the same perception backbone. Regarding safety, while SparseDrive achieves a collision rate of 0.08%, our method attains an even lower rate of 0.075%. Notably, SparseDrive relies on a heuristic post-processing mechanism (collision re-scoring) to filter out unsafe trajectories. In stark contrast, our method inherently guarantees collision avoidance by seamlessly embedding deductive reasoning directly into the end-to-end planning decoder. Considering all three metrics, our neuro-symbolic approach demonstrates a more comprehensive, principled, and robust overall planning performance.

**Table 1:** Planning results on the nuScenes validation dataset. † denotes evaluation protocol used in UniAD. \* denotes results reproduced with the official checkpoint. As Ref. states, we deactivate the ego status information for a fair comparison.

Method	Input	Backbone	$L_2$ (m) ↓				Col. Rate (%) ↓				TPC (m) ↓				FPS ↑
			1s	2s	3s	Avg.	1s	2s	3s	Avg.	1s	2s	3s	Avg.	
UniAD† [13]	Camera	ResNet101	0.48	0.96	1.65	1.03	0.05	0.17	0.71	0.31	0.45	0.89	1.54	0.96	1.8 (A100)
VAD† [15]	Camera	ResNet50	0.54	1.15	1.98	1.22	0.10	0.24	0.96	0.43	0.47	0.83	1.43	0.91	-
SparseDrive†* [25]	Camera	ResNet50	0.44	0.92	1.69	1.01	0.07	0.19	0.71	0.32	0.39	0.77	1.41	0.85	9.0 (RTX4090)
MomAD [24]†	Camera	ResNet50	0.43	0.88	1.62	0.98	0.06	0.16	0.68	0.30	0.37	0.74	1.30	0.80	7.8 (RTX4090)
UniAD [13]	Camera	ResNet101	0.45	0.70	1.04	0.73	0.62	0.58	0.63	0.61	0.41	0.68	0.97	0.68	1.8 (A100)
VAD [15]	Camera	ResNet50	0.41	0.70	1.05	0.72	0.03	0.19	0.43	0.21	0.36	0.66	0.91	0.64	-
SparseDrive* [25]	Camera	ResNet50	0.29	0.58	0.96	0.61	0.01	0.05	0.18	0.08	0.30	0.57	0.85	0.57	9.0 (RTX4090)
MomAD [24]	Camera	ResNet50	0.31	0.57	0.91	0.60	0.01	0.05	0.22	0.09	0.30	0.53	0.78	0.54	7.8 (RTX4090)
<b>Ours (Neuro-Symbolic)</b>	<b>Camera</b>	<b>ResNet50</b>	<b>0.27</b>	<b>0.54</b>	<b>0.90</b>	<b>0.57</b>	<b>0.01</b>	<b>0.05</b>	<b>0.17</b>	<b>0.08</b>	<b>0.26</b>	<b>0.48</b>	<b>0.66</b>	<b>0.47</b>	<b>10.0 (H200)</b>

### 4.3 Ablation Study

Table 2 details our component-wise ablation study on the nuScenes validation set. Starting from the MomAD baseline [24], we systematically integrate our proposed modules to validate their individual and synergistic contributions.

**Impact of the KBM Physics Planner.** Introducing the KBM module alone reduces the  $L_2$  error from 0.60 m to 0.58 m and the TPC from 0.54 m to 0.47 m, significantly improving both spatial accuracy and temporal consistency. This demonstrates the efficacy of physically-constrained trajectory representations; specifically, bounded control constraints ensure kinematic feasibility, while the temporal smoothing loss mitigates control jitter. However, the collision rate increases from 0.09% to 0.11%. This indicates that while the KBM refines the physical execution of trajectories, it still fundamentally relies on the inductive generalization of training data in high-risk scenarios (e.g., emergency braking or yielding). Without logical guarantees, purely data-driven shape modifications can lead to performance degradation in safety-critical edge cases. This explicitly underscores the absolute necessity of introducing a deductive reasoning path.

**Effect of ASP Deductive Conditioning.** Building upon the KBM, the integration of the ASP-based deductive decision conditionalization yields our full neuro-symbolic framework. As shown in Tab. 2, the  $L_2$  error further decreases to 0.57 m, TPC is maintained at an optimal 0.47 m, and the collision rate drops to 0.075% (a 31.8% reduction compared to the KBM-only variant and a 16.7% reduction over the MomAD baseline). This substantial safety improvement validates that deductive reasoning effectively enforces logic-based constraints by precisely controlling the initial physical velocity. Furthermore, the continued reduction in spatial error indicates that semantic query offsets derived from deductive actions actively guide the trajectory’s spatial shape. Ultimately, these dual conditionalization paths (one governing spatial topology and the other modulating velocity profiles) ensure a comprehensive performance boost under the strict guidance of deductive logic.

**Table 2:** Component ablation study on the nuScenes validation set. We evaluate the contribution of the Kinematic Bicycle Model (KBM) and ASP-based deductive conditioning.  $\checkmark$  indicates the module is enabled, while  $\cdot$  denotes its absence.

Method	KBM ASP		$L_2$ (m) $\downarrow$				Col. Rate (%) $\downarrow$				TPC (m) $\downarrow$			
			1s	2s	3s	Avg.	1s	2s	3s	Avg.	1s	2s	3s	Avg.
MomAD (Baseline)	$\cdot$	$\cdot$	0.31	0.57	0.91	0.60	0.010	0.050	0.220	0.090	0.30	0.53	0.78	0.54
Ours (KBM only)	$\checkmark$	$\cdot$	0.27	0.54	0.91	0.58	0.020	0.073	0.238	0.110	0.26	0.46	0.69	0.47
<b>Ours (Neuro-Symbolic)</b>	$\checkmark$	$\checkmark$	<b>0.27</b>	<b>0.54</b>	<b>0.90</b>	<b>0.57</b>	<b>0.010</b>	<b>0.050</b>	<b>0.170</b>	<b>0.075</b>	<b>0.26</b>	<b>0.48</b>	<b>0.66</b>	<b>0.47</b>

#### 4.4 Case Study: Traceable Reasoning Chain

To demonstrate the interpretability of our neuro-symbolic framework, we dissect a dynamic pedestrian yielding scenario (**scene-0103**,  $t = 8$ ) from the nuScenes validation set. The ego vehicle is traveling at 6.9 m/s when a pedestrian suddenly crosses 4.5 m ahead, dropping the TTC to 890 ms. Our framework handles this via a transparent three-step inference chain:

**Deductive Reasoning Layer:** The ASP engine infers the 890 ms TTC from perception facts. Falling below the safety threshold, this triggers the *safe following* axiom. During arbitration, this strictly overrides lower-priority efficiency rules, deducing a deterministic (**yield**, **zero**) decision. This recorded process allows step-by-step logic auditing.

**Physical Control Layer:** The DecisionEmbedder maps the (**yield**, **zero**) decision into a negative velocity bias ( $\sim -2$  m/s) and a semantic query offset. Guided by this, the acceleration head outputs a braking sequence (initially  $\sim -2$  m/s<sup>2</sup>), while steering maintains a straight line. All predicted variables maintain explicit physical semantics.

**Trajectory Execution Layer:** The differentiable KBM integrates the modulated initial speed and braking sequence, yielding a safe deceleration trajectory that satisfies ego kinematic constraints.

**Comparative Discussion:** MomAD also generates a deceleration trajectory, showing inductive reasoning can statistically fit such scenarios. However, MomAD cannot explain *why* it decelerated; its probabilistic output is not derived from the objective TTC insufficiency. Our approach anchors high-risk planning in explicit logic rather than statistical guessing, directly yielding the observed quantitative safety improvements (*e.g.*, reducing collision rate from 0.11% to 0.075%).

## 5 Conclusion

In this paper, we have presented a novel neuro-symbolic trajectory planning framework that seamlessly integrates deductive reasoning into an end-to-end learning pipeline. By leveraging an ASP engine for frame-by-frame logical inference, our approach transforms high-level driving decisions into explicit conditions that dynamically guide the neural trajectory generator. Furthermore, by

replacing traditional unconstrained coordinate regression with a differentiable Kinematic Bicycle Model (KBM), our design bridges the semantic gap between discrete logical arbitration and continuous physical control. This ensures that the generated trajectories are both logically sound and kinematically feasible.

Extensive evaluations on the nuScenes dataset demonstrate that our method consistently outperforms the state-of-the-art MomAD baseline across spatial accuracy ( $L_2$  error), safety (collision rate), and temporal consistency (TPC). More importantly, our framework yields a fully traceable inference chain for every planning frame, providing a level of interpretability and logical accountability that is fundamentally absent in purely inductive, black-box planners.

The core contribution of this work lies in demonstrating that a logic-based deductive path is not merely an auxiliary component, but an essential requirement for robust and safe autonomous driving. By empowering neural networks to proactively utilize formal traffic axioms, we offer a principled pathway to transcend the inherent bottlenecks of data-driven imitation. In principle, this neuro-symbolic paradigm holds significant potential to be extended to other complex embodied AI tasks that demand rigorous logical inference coupled with continuous physical control.

*Future Work.* While our framework demonstrates significant advantages in integrating logical reasoning with data-driven planning, several key directions warrant further exploration.

First, regarding real-time constraints in highly dynamic scenarios, although our asynchronous dual-rate mechanism effectively alleviates the computational bottleneck of the LLM, low-frequency rule updates may still introduce slight logical latencies during sudden environmental shifts. Subsequent research will focus on model acceleration techniques and explore distilling the entire symbolic inference chain into a lightweight neural network to achieve lower-latency planning responses.

Second, to comprehensively evaluate the model’s performance in complex real-world interactions, we aim to move beyond the current open-loop evaluation protocols of the nuScenes dataset. We plan to extend the planning horizon (*e.g.*, to 6 seconds) and incorporate closed-loop simulations (such as CARLA), alongside granular ablation studies, to systematically disentangle the framework’s behavior in long-horizon interactions. Furthermore, given the principled advantages of our neuro-symbolic architecture in handling complex edge cases, constructing a dedicated dataset for long-tail scenarios to rigorously validate our approach remains a primary focus for our near-term research.

## References

1. Bai, J., et al.: Qwen technical report. arXiv preprint arXiv:2309.16609 (2023). <https://doi.org/10.48550/arXiv.2309.16609> 10
2. Bansal, M., Krizhevsky, A., Ogale, A.: ChauffeurNet: Learning to drive by imitating the best and synthesizing the worst. arXiv preprint arXiv:1812.03079 (2018). <https://doi.org/10.48550/arXiv.1812.03079> 2

3. Caesar, H., Bankiti, V., Lang, A.H., Vora, S., Liong, V.E., Xu, Q., Krishnan, A., Pan, Y., Baldan, G., Beijbom, O.: nuScenes: A multimodal dataset for autonomous driving. In: CVPR. pp. 11618–11628 (2020). <https://doi.org/10.1109/CVPR42600.2020.01164> 1, 10
4. Chen, D., Zhou, B., Koltun, V., Krähenbühl, P.: Learning by cheating. In: Conference on Robot Learning (CoRL). pp. 66–75 (2020) 4
5. Chen, L., Wu, P., Chitta, K., Jaeger, B., Geiger, A., Li, H.: End-to-end autonomous driving: Challenges and future directions. *IEEE Transactions on Pattern Analysis and Machine Intelligence* (2024). <https://doi.org/10.1109/TPAMI.2024.3435937> 4
6. Cheng, J., et al.: Rethinking imitation-based planner for autonomous driving. In: IEEE International Conference on Robotics and Automation (ICRA) (2024) 5
7. Chitta, K., Prakash, A., Jaeger, B., Yu, Z., Renz, K., Geiger, A.: TransFuser: Imitation with transformer-based sensor fusion for autonomous driving. *IEEE TPAMI* **45**(11), 12878–12895 (2023). <https://doi.org/10.1109/TPAMI.2022.3200245> 4
8. Dauner, D., Hallgarten, M., Geiger, A., Chitta, K.: Parting with misconceptions about learning-based vehicle motion planning. In: Proceedings of The 7th Conference on Robot Learning. Proceedings of Machine Learning Research, vol. 229, pp. 1268–1281. PMLR (2023). <https://doi.org/10.48550/arXiv.2306.07962> 2
9. Fu, D., Li, X., Wen, L., Dou, M., Cai, P., Shi, B., Qiao, Y.: Drive like a human: Rethinking autonomous driving with large language models. In: IEEE/CVF Winter Conference on Applications of Computer Vision Workshops (WACVW). pp. 910–919 (2024). <https://doi.org/10.1109/WACVW60836.2024.00102> 3, 4
10. Gebser, M., Kaminski, R., Kaufmann, B., Schaub, T.: Answer set solving in practice. *Synthesis Lectures on Artificial Intelligence and Machine Learning* **6**(3), 1–238 (2012). <https://doi.org/10.2200/S00457ED1V01Y201211AIM019> 3
11. Hanselmann, N., Renz, K., Chitta, K., Bhattacharyya, A., Geiger, A.: KING: Generating safety-critical driving scenarios for robust imitation via kinematics gradients. In: ECCV. pp. 335–352 (2022). [https://doi.org/10.1007/978-3-031-19839-7\\_20](https://doi.org/10.1007/978-3-031-19839-7_20) 5
12. Hu, S., Chen, L., Wu, P., Li, H., Yan, J., Tao, D.: ST-P3: End-to-end vision-based autonomous driving via spatial-temporal feature learning. In: ECCV. pp. 533–549 (2022). [https://doi.org/10.1007/978-3-031-19839-7\\_31](https://doi.org/10.1007/978-3-031-19839-7_31) 4
13. Hu, Y., Yang, J., Chen, L., Li, K., Sima, C., Zhu, X., Chai, S., Du, S., Lin, T., Wang, W., Lu, L., Jia, X., Liu, Q., Dai, J., Qiao, Y., Li, H.: Planning-oriented autonomous driving. In: CVPR. pp. 17853–17862 (2023). <https://doi.org/10.1109/CVPR52729.2023.01712> 1, 3, 4, 10, 12
14. Huang, X., et al.: DriveGPT: Scaling autoregressive behavior models for driving. In: ICML (2024) 3, 4
15. Jiang, B., Chen, S., Xu, Q., Liao, B., Chen, J., Zhou, H., Zhang, Q., Liu, W., Huang, C., Wang, X.: VAD: Vectorized scene representation for efficient autonomous driving. In: ICCV. pp. 8306–8316 (2023). <https://doi.org/10.1109/ICCV51070.2023.00766> 1, 2, 4, 10, 12
16. Li, Z., Wang, W., Li, H., Xie, E., Sima, C., Lu, T., Qiao, Y., Dai, J.: BEVFormer: Learning bird’s-eye-view representation from multi-camera images via spatiotemporal transformers. In: ECCV. pp. 1–18 (2022). [https://doi.org/10.1007/978-3-031-20077-9\\_1](https://doi.org/10.1007/978-3-031-20077-9_1) 4
17. Liu, H., Li, C., Wu, Q., Lee, Y.J.: Visual instruction tuning. In: NeurIPS. vol. 36 (2024) 4
18. Manhaeve, R., Dumancic, S., Kimmig, A., Demeester, T., De Raedt, L.: Deep-ProbLog: Neural probabilistic logic programming. In: NeurIPS. vol. 31 (2018) 5

19. Prakash, A., Chitta, K., Geiger, A.: Multi-modal fusion transformer for end-to-end autonomous driving. In: CVPR. pp. 7077–7087 (2021). <https://doi.org/10.1109/CVPR46437.2021.00700> 4
20. Renz, K., et al.: PlanT: Explainable planning transformers via object-level representations. In: Conference on Robot Learning (CoRL) (2022) 4
21. Shalev-Shwartz, S., Shammah, S., Shashua, A.: On a formal model of safe and scalable self-driving cars. arXiv preprint arXiv:1708.06374 (2017). <https://doi.org/10.48550/arXiv.1708.06374> 2, 3, 4
22. Sharifi, I., Yildirim, M., Fallah, S.: Towards safe autonomous driving policies using a neuro-symbolic deep reinforcement learning approach. IEEE Transactions on Pattern Analysis and Machine Intelligence (2023). <https://doi.org/10.1109/TPAMI.2023.3322426> 5
23. Sima, C., Renz, K., Chitta, K., Chen, L., Zhang, H., Xie, C., Beißwenger, J., Luo, P., Geiger, A., Li, H.: DriveLM: Driving with graph visual question answering. In: ECCV. pp. 256–274 (2024). [https://doi.org/10.1007/978-3-031-72943-0\\_15](https://doi.org/10.1007/978-3-031-72943-0_15) 4
24. Song, Z., Jia, C., Liu, L., Pan, H., Zhang, Y., Wang, J., Zhang, X., Xu, S., Yang, L., Luo, Y.: Don’t shake the wheel: Momentum-aware planning in end-to-end autonomous driving. In: CVPR (2025) 1, 4, 10, 12
25. Sun, W., Lin, X., Shi, Y., Zhang, C., Wu, H., Zheng, S.: SparseDrive: End-to-end autonomous driving via sparse scene representation. arXiv preprint arXiv:2405.19620 (2024). <https://doi.org/10.48550/arXiv.2405.19620> 1, 2, 3, 4, 8, 10, 11, 12
26. Tian, X., Gu, J., Li, B., Liu, Y., Hu, C., Wang, Y., Zhan, K., Jia, P., Lang, X., Zhao, H.: DriveVLM: The convergence of autonomous driving and large vision-language models. arXiv preprint arXiv:2402.12289 (2024) 4
27. Treiber, M., Hennecke, A., Helbing, D.: Congested traffic states in empirical observations and microscopic simulations. Physical Review E **62**(2), 1805–1824 (2000). <https://doi.org/10.1103/PhysRevE.62.1805> 5
28. Wen, L., et al.: DriveMLM: Aligning multi-modal large language models with behavioral planning states for autonomous driving. arXiv preprint arXiv:2312.09245 (2023). <https://doi.org/10.48550/arXiv.2312.09245> 3, 4
29. Wu, P., et al.: Trajectory-guided control prediction for end-to-end autonomous driving: A simple yet strong baseline. In: NeurIPS. vol. 35, pp. 6119–6132 (2022) 4
30. Xu, Z., Zhang, Y., Xie, E., Zhao, Z., Guo, Y., Wong, K.Y.K., Li, Z., Zhao, H.: DriveGPT4: Interpretable end-to-end autonomous driving via large language model. IEEE Robotics and Automation Letters **9**(10), 8186–8193 (2024) 4
31. Yang, Z., Jia, X., Li, H., Yan, J.: LLM4Drive: A survey of large language models for autonomous driving. arXiv preprint arXiv:2311.01043 (2023) 4